Electronic Supplementary Information (ESI)

Effect of Incorporating Regioisomers and Flexible Rotors to Direct Aggregation Induced Emission and Achieve Stimuli-responsive Luminogens, Security Inks and Chemical Warfare Agent Sensors

Laxmi Raman Adil[a] and Parameswar Krishnan Iyer[a,b]*

[a]Department of Chemistry, [b]Center for Nanotechnology, Indian Institute of Technology Guwahati, Guwahati-781039, Assam, India.

Corresponding author:
*E-mail: pki@iitg.ac.in;

Fax: +91 361 258 2349 (Prof. P. K. Iyer).

Table of Contents

1. Materials and instrumentation

Fluorene, 4-pyridinylboronic acid, potassium tert-butoxide, 4-bromobenzaldehyde, 2-bromobenzaldehyde, 4-bromobenzyl bromide, triethylphosphite (TEP), dimethyl methylphosphonat (DMMP), diethylchlorophosphate (DCP), tributylphosphate (TBP), chlorodiphenylphosphine (Ph_2PCl) were purchased from Sigma Aldrich. Benzophenone, tetrahydrofuran (THF), chloroform were bought from Zenith India. All mentioned chemicals were received commercially and used without any further purification. HPLC grade solvents from Zenith India. THF was used for the preparation of stock solutions and photophysical experiments were performed by using THF and Milli-Q water. All the reactions which were moisture and air sensitive were performed under argon atmosphere by using the standard technique. ^{1}H NMR (400 MHz) and ^{13}C NMR (100 MHz) spectra were obtained on Varian-AS400 spectrometer. The photophysical studies of PN derivatives were done in HPLC grade solvents (DCM, DMSO, THF, Toluene) and Milli-Q water. The standard solution of 1PN, 1PON and 3PN were prepared at a one mM concentration in THF solvent. UV vis. spectra and Photoluminescence (PL) were recorded on PerkinElmer Lambda and Horiba Fluoromax-4 using 10 mm path length quartz cuvettes with a 3 nm slit width at 298 K.

2. Nerve agent simulants

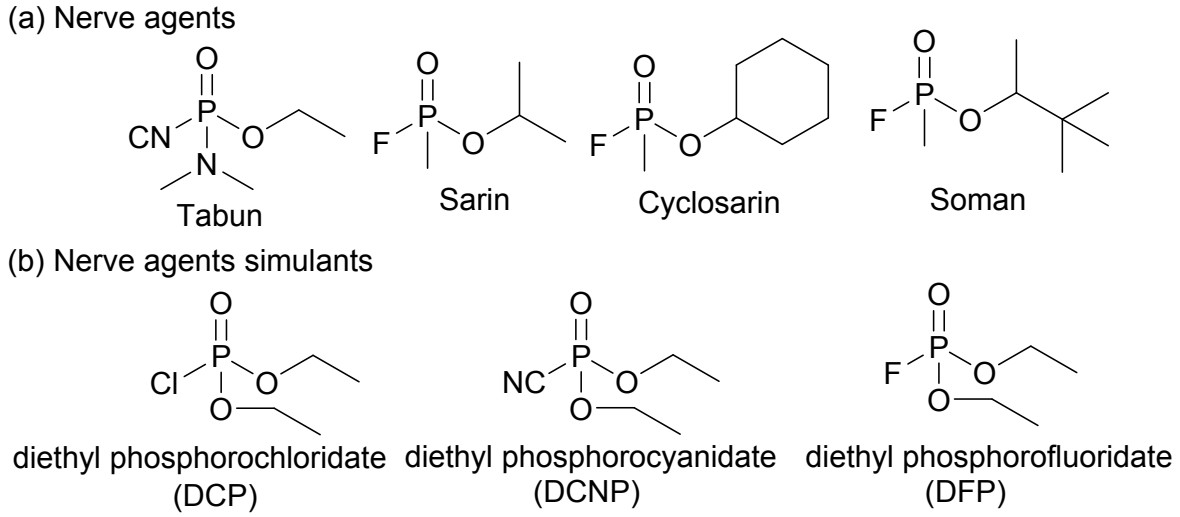

Fig. S1 Chemical structure of tabun, sarin, cyclosarin, soman (nerve agents) and DCP, DCNP, DFP (nerve agent simulants).

3. Synthesis scheme

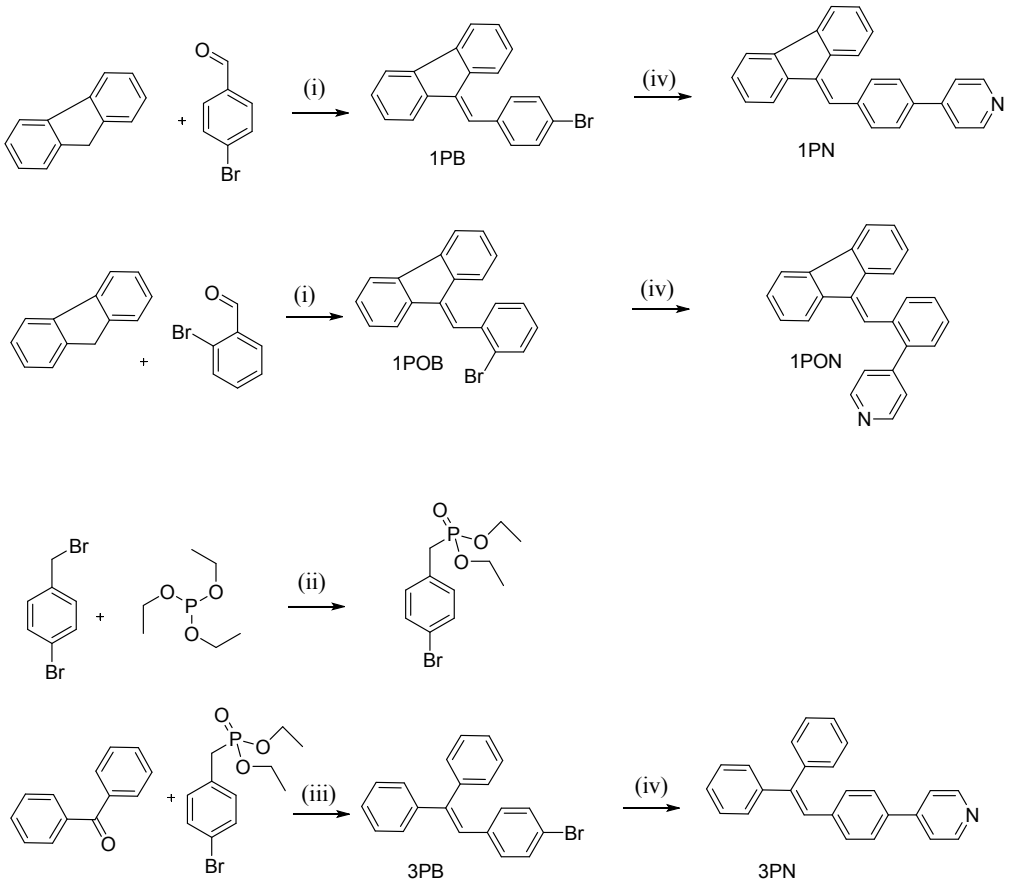

Scheme S1 (i) K^{t}Bu, Ethanol, 80°C, 12 h (ii) THF, 80°C, 10 h (iii) K^{t}Bu, THF, RT, 12 h (iv) 4-pyridinyl boronic acid, $Pd(PPh_3)_4$, K_2CO_3, THF:H_2O, 80°C, 24 h.

4. Synthesis Methods

<u>The synthesis procedure of 1PBr</u>

A mixture of fluorene (0.166 g, 1eq.) and potassium tert-butoxide (0.137 g, 1.2 eq.) was dissolved in 10 mL absolute ethanol and refluxed for 1 hour than 4 bromo benzaldehyde (0.185 g, 1 eq.) was added into resulting mixture then it was refluxed for 24 hours. The solvent was removed by rotary evaporator and the compound was extracted with dichloromethane (DCM) and water. Pure compound 1PBr was collected from silica column chromatography by taking hexane as eluent. (yellow solid, 0.245 g, 73% yield).

1PBr ^{1}H NMR (400 MHz, $CDCl_3$, δ ppm): 7.08 (t, 1H), 7.32 (t, 2H), 7.39 (t, 1H) 7.45 (d, 2H), 7.51 (d, 1H) 7.58 (m, 3H), 7.70 (d, 2H) 7.76 (d, 1H).

1PBr ^{13}C NMR (100.00 MHz, $CDCl_3$, δ ppm) 119.77, 119.97, 120.39, 122.17, 124.43, 125.78, 126.88, 127.19, 128.56, 128.92, 131.07, 131.84, 135.86, 136.35, 137.12, 139.31, 141.47.

The synthesis procedure of 1POBr

1POBr was synthesized by the above prescribed method. (yellow solid, 0.260 g, 78.07% yield).

1POBr ^{1}H NMR (400 MHz, $CDCl_3$, δ ppm): 7.17 (t, 1H), 7.39 (m, 6H), 7.61 (d, 1H) 7.70 (d, 1H), 7.77 (m, 2H) 7.92 (m, 1H), 8.03 (d, 1H).

1POBr ^{13}C NMR (100.00 MHz, $CDCl_3$, δ ppm) 141.25, 139.61, 139.24, 137.25, 136.77, 136.35, 133.54, 129.65, 128.31, 128.23, 127.81, 127.40, 127.17, 126.87, 125.26, 124.59, 120.46, 120.18, 119.82.

The synthesis procedure of 3PBr

Into condenser fitted round bottom flask 1-bromo-4-(bromomethyl)benzene (0.249 g, 1 mmol), triethyl phosphite (0.5 mL) in 10 ml of THF refluxed for 10 hours then benzophenone (0.182 g, 1 mmol) and potassium tertiary butoxide (0.112 g, 1 mmol) added and the reaction stirred at room temperature for 12 hours. The reaction mixture was quenched and workup performed by using DCM and water. Pure product 3PBr was collected by silica column chromatography by taking hexane an eluent. (white solid, 0.215 g, 64.56% yield.

3PBr ^{1}H NMR (400 MHz, $CDCl_3$, δ ppm): 6.87 (m, 1H), 6.89 (m, 2H), 7.19 (m, 2H), 7.24 (m, 1H) 7.32 (m, 8H).

3PBr ^{13}C NMR (100.00 MHz, $CDCl_3$, δ ppm) 120.70, 126.93, 127.73, 127.78, 127.88, 128.40, 128.90, 130.40, 131.19, 131.23, 136.47, 140.08, 143.20, 143.58.

The synthesis procedure of 1PN

9-(4-bromobenzylidene)-9H-fluorene (0.332 g, 1 eq.), phenylboronic acid (0.134 g, 1.1 eq.), tetrakis(triphenylphosphine) palladium (0) (0.015 mmol) were taken in inert medium (argon gas) then 10 ml THF and aqueous K_2CO_3 (2M) was added. The reaction was refluxed for overnight. The reaction was quenched and workup performed by DCM and water. Pure product collected by silica column chromatography (yellow crystalline solid, 0.214 g,64.56% yield). Yellow color crystals with blocked shaped were growth in 9:1 methanol and DCM by slow evaporation.

1PN ^{1}H NMR (400 MHz, $CDCl_3$, δ ppm): 7.08 (t, 1H), 7.36 (m, 3H), 7.61 (m, 3H), 7.74 (m, 7H), 7.79 (m, 1H), 8.70 (d, 2H).

1PN ^{13}C NMR (100.00 MHz, $CDCl_3$, δ ppm) 119.80, 119.99, 120.45, 121.58, 124.49, 126.27, 126.85, 127.19, 127.23, 128.59, 128.95, 130.30, 136.46, 137.25, 137.64, 137.96, 139.35, 139.46, 141.54, 147.77, 150.51.

The synthesis procedure of 1PON

Synthesis of **1PON** was done by the above prescribed method. (Yellow solid, 0.225 g, 67.56 yield). Yellow color crystals with rectangular shaped were growth in toluene and DCM by slow evaporation.

1PON ^{1}H NMR (400 MHz, $CDCl_3$, δ ppm): 7.09 (t, 1H), 7.27 (m, 1H), 7.36 (m, 5H), 7.54 (m, 4H), 7.58 (d, 1H), 7.73 (t, 2H), 7.77 (d, 1H).

1PON ^{13}C NMR (100.00 MHz, $CDCl_3$, δ ppm) 119.72, 120.01, 120.54, 124.42, 124.46, 126.52, 126.88, 127.18, 128.50, 128.68, 128.87, 129.00, 129.74, 131.34, 135.15, 136.63, 137.38, 138.65, 139.07, 139.16, 141.47, 148.42, 149.76.

The synthesis procedure of 3PN

Synthesis of **3PN** was done by the above prescribed method. (white solid, 0.220 g, 66.06 yield). Colorless crystals with needle-shaped were growth in 9:1 methanol and DCM mixture by slow evaporation.

3PN ^{1}H NMR (400 MHz, $CDCl_3$, δ ppm): 7.00 (s, 1H), 7.12 (d, 2H), 7.24 (m, 2H), 7.35 (m, 8H), 7.44 (d, 4H), 8.60 (d, 2H).

3PN ^{13}C NMR (100.00 MHz, $CDCl_3$, δ ppm): 121.31, 121.75, 126.57, 127.10, 127.26, 127.74, 127.77, 127.89, 128.37, 128.89, 129.17, 129.22, 130.32, 130.40, 136.02, 138.47, 140.23, 143.18, 143.84, 247.73, 150.29.

5. ^{1}H, ^{13}C NMR and Mass Spectra

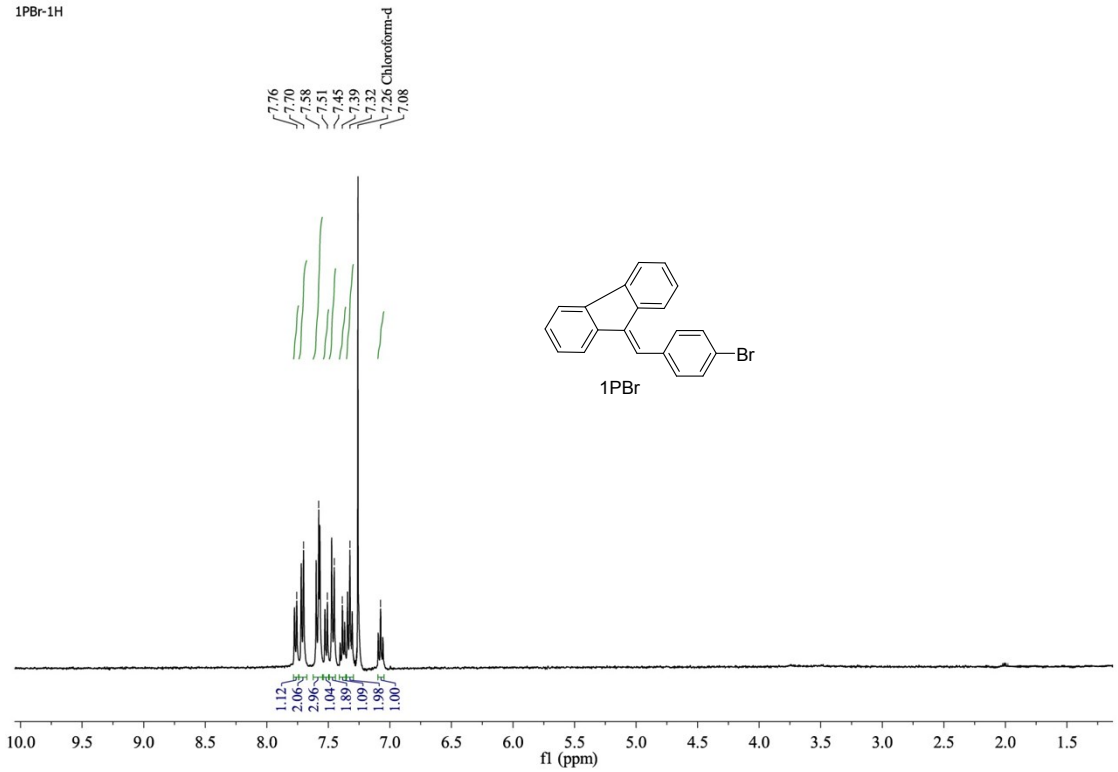

Fig. S2 ^{1}H NMR spectra of 1PBr in $CDCl_3$ solvent.

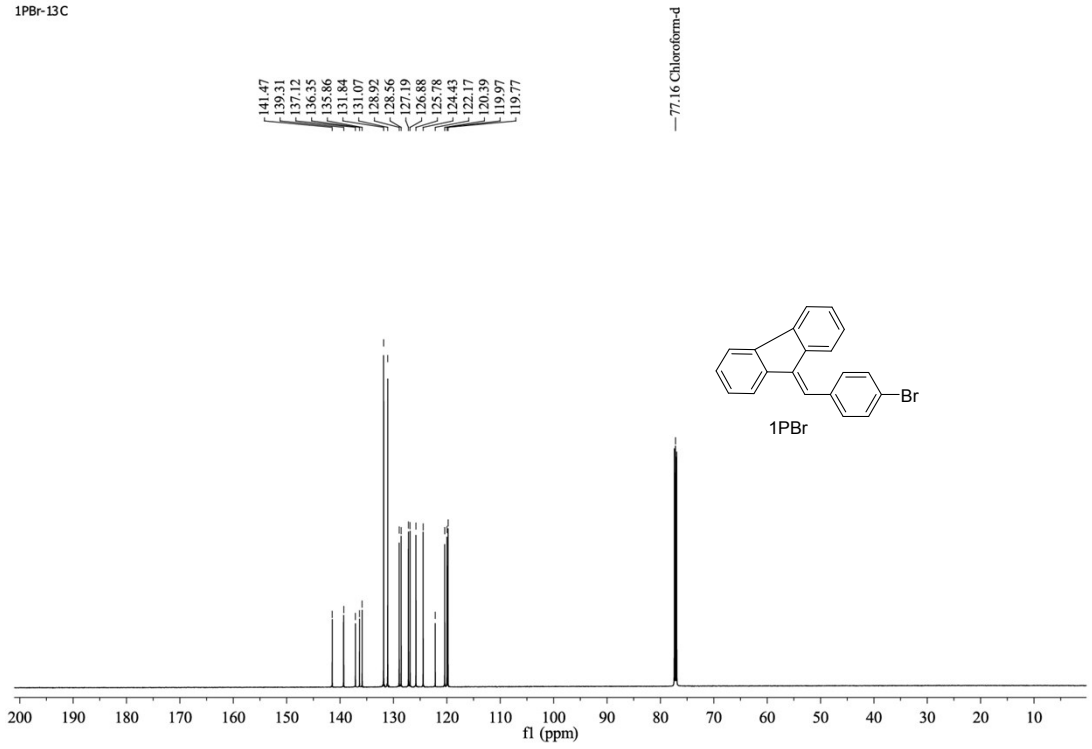

Fig. S3 ^{13}C NMR spectra of 1PBr in $CDCl_3$ solvent.

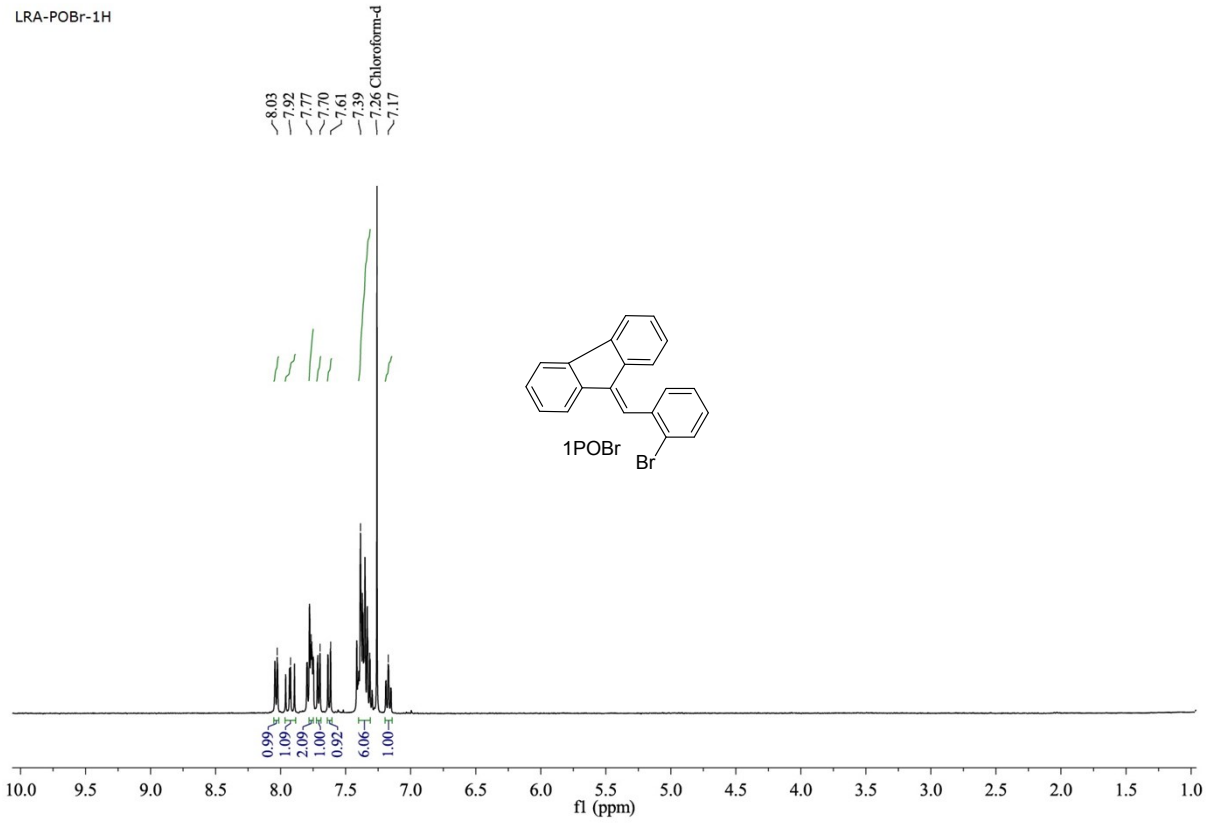

Fig. S4 ^{1}H NMR spectra of 1POBr in $CDCl_3$ solvent.

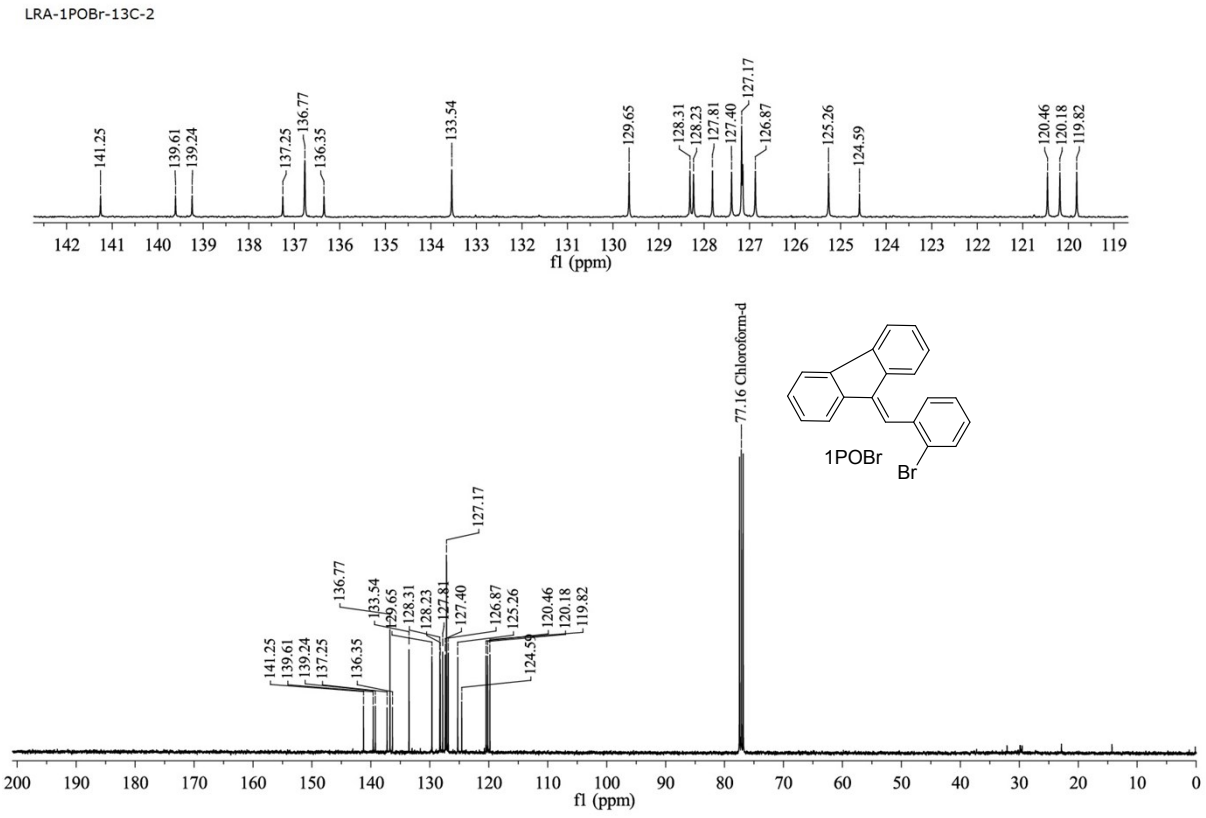

Fig. S5 ^{13}C NMR spectra of 1POBr in $CDCl_3$ solvent.

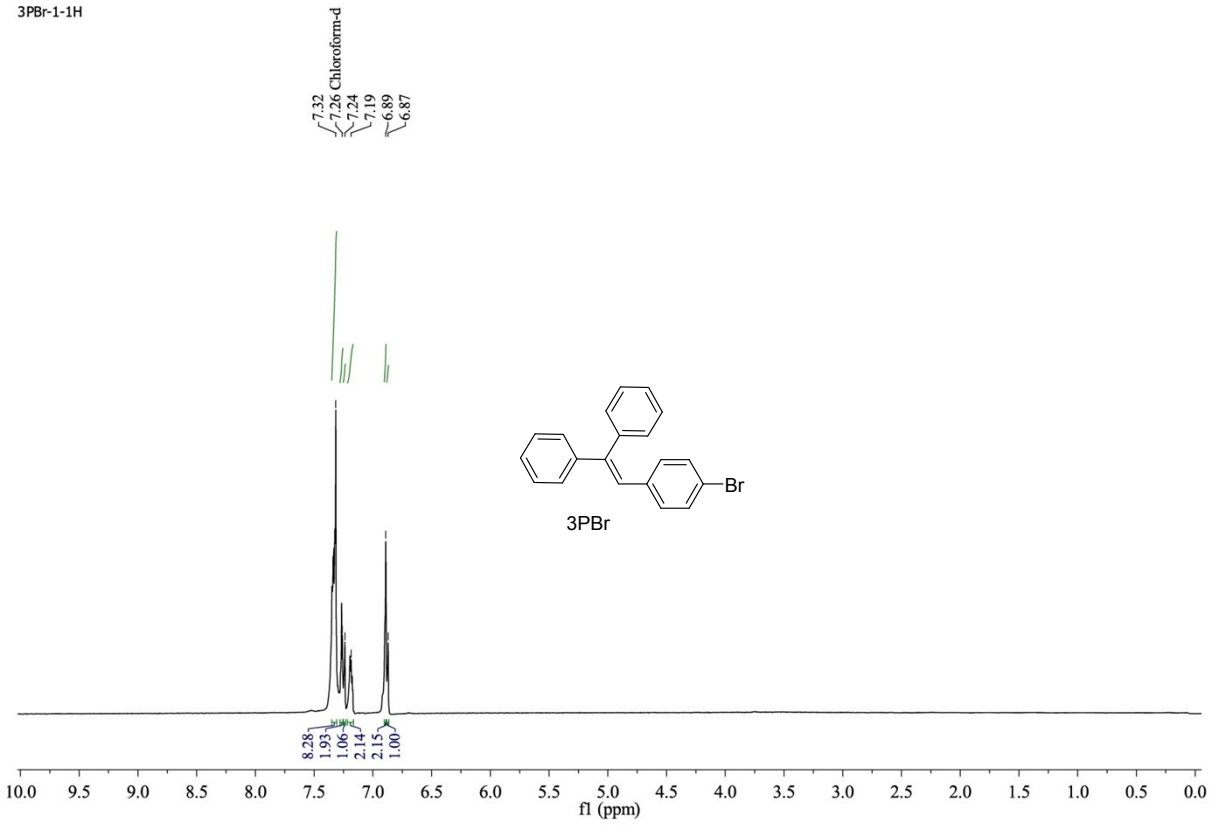

Fig. S6 ^{1}H NMR spectra of 3PBr in $CDCl_3$ solvent.

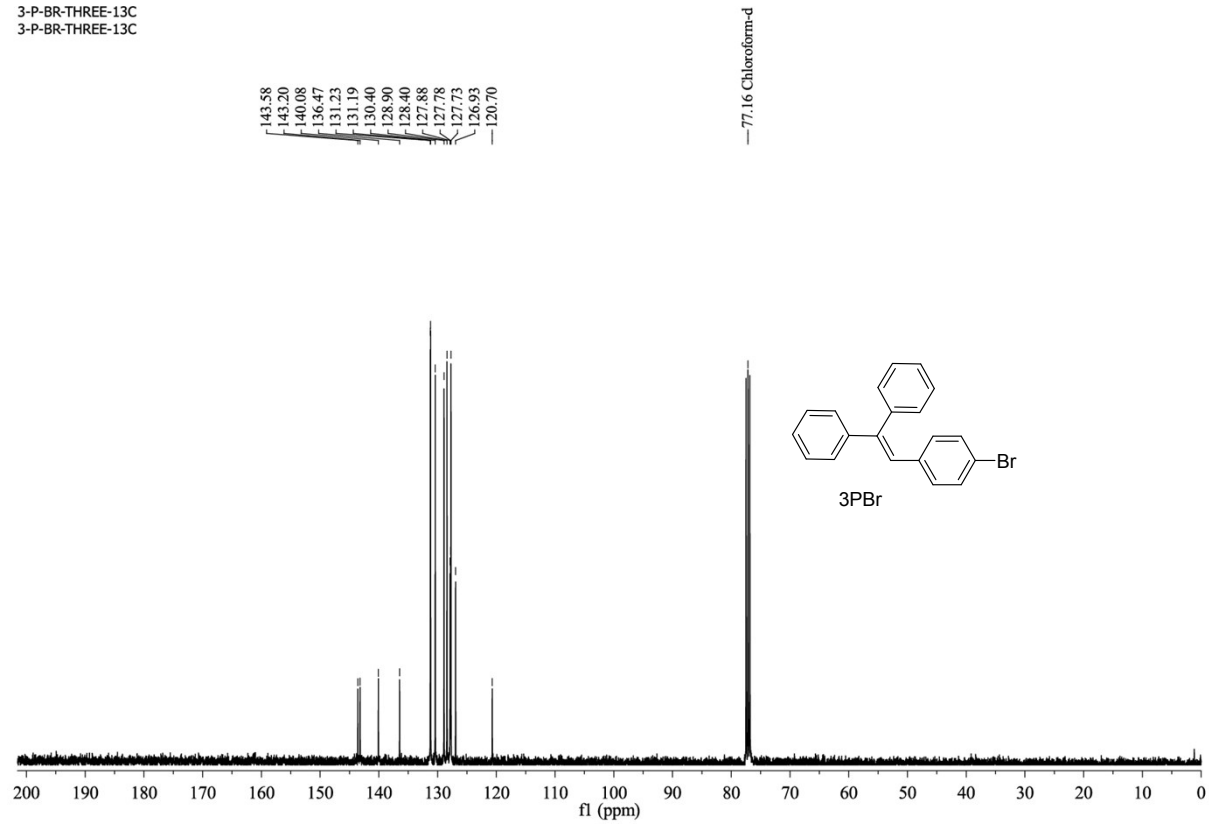

Fig. S7 ^{13}C NMR spectra of 3PBr in $CDCl_3$ solvent.

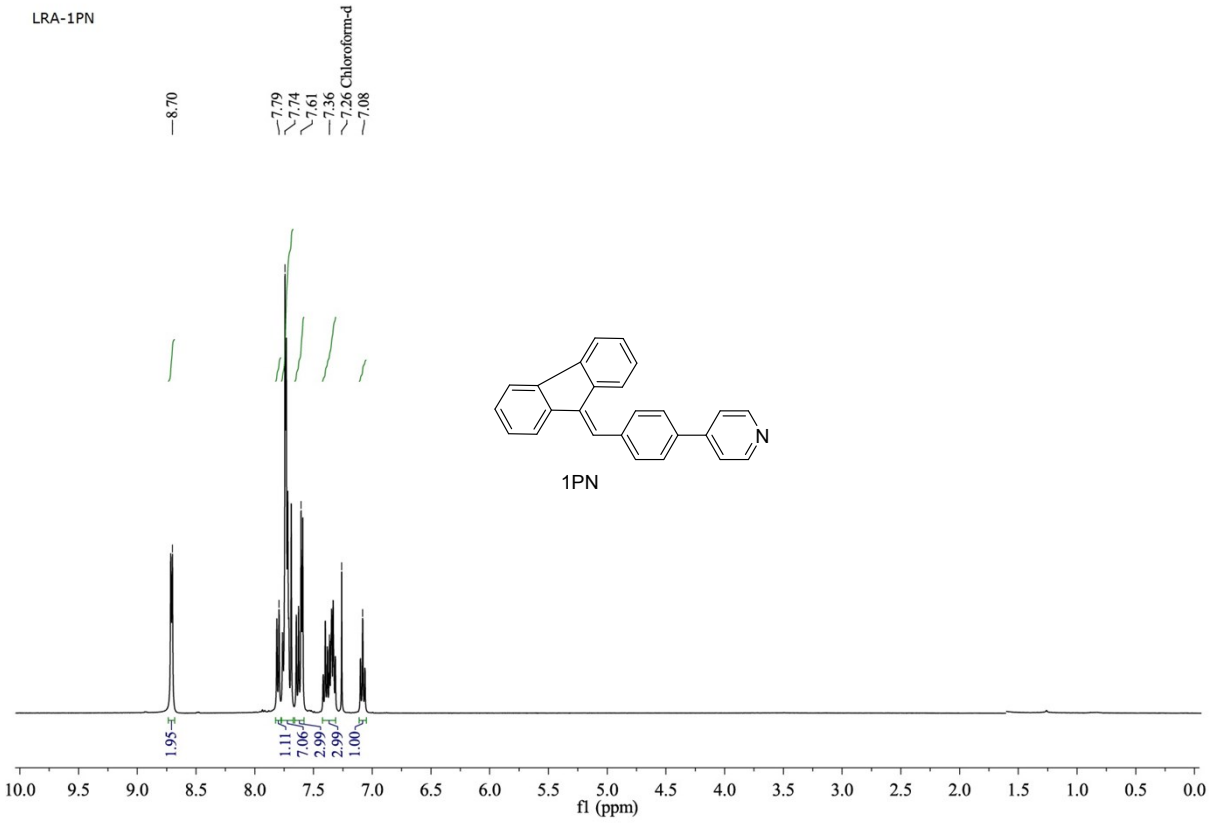

Fig. S8 ^{1}H NMR spectra of **1PN** in $CDCl_3$ solvent.

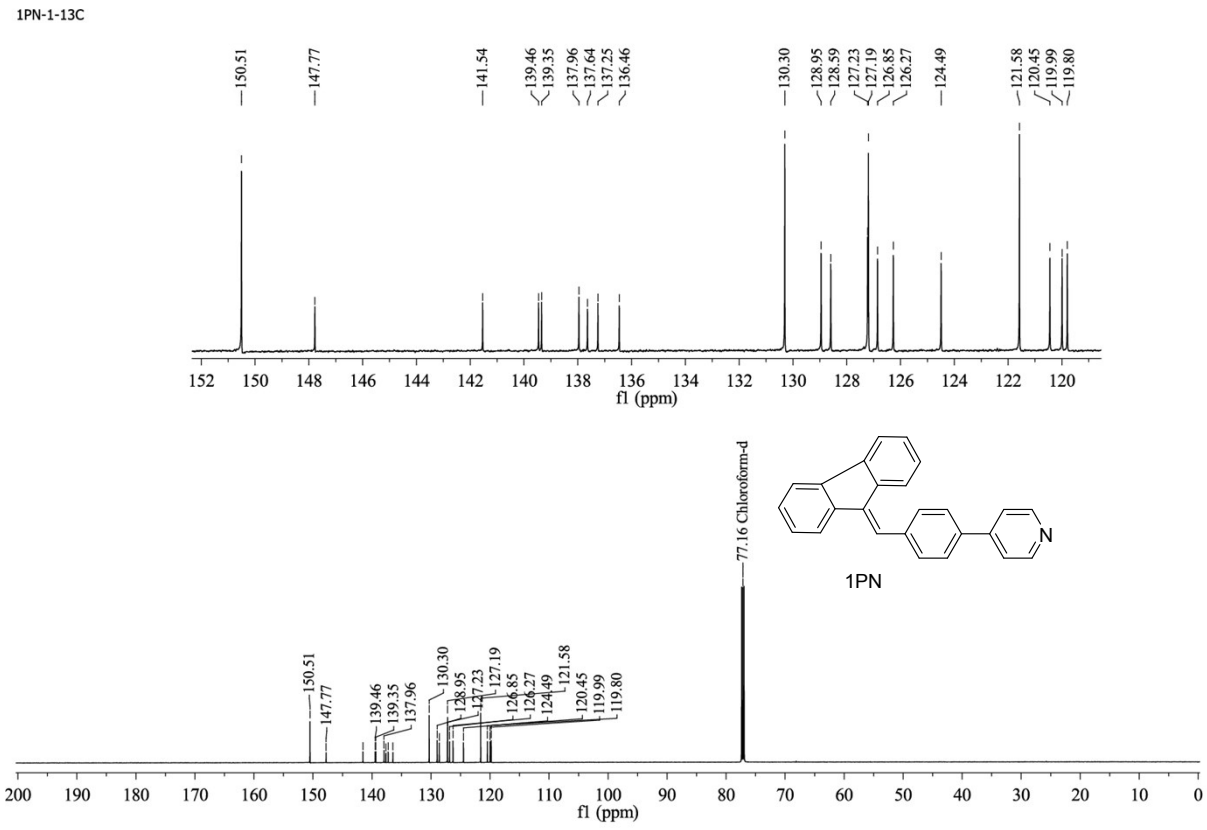

Fig. S9 ^{13}C NMR spectra of **1PN** in $CDCl_3$ solvent.

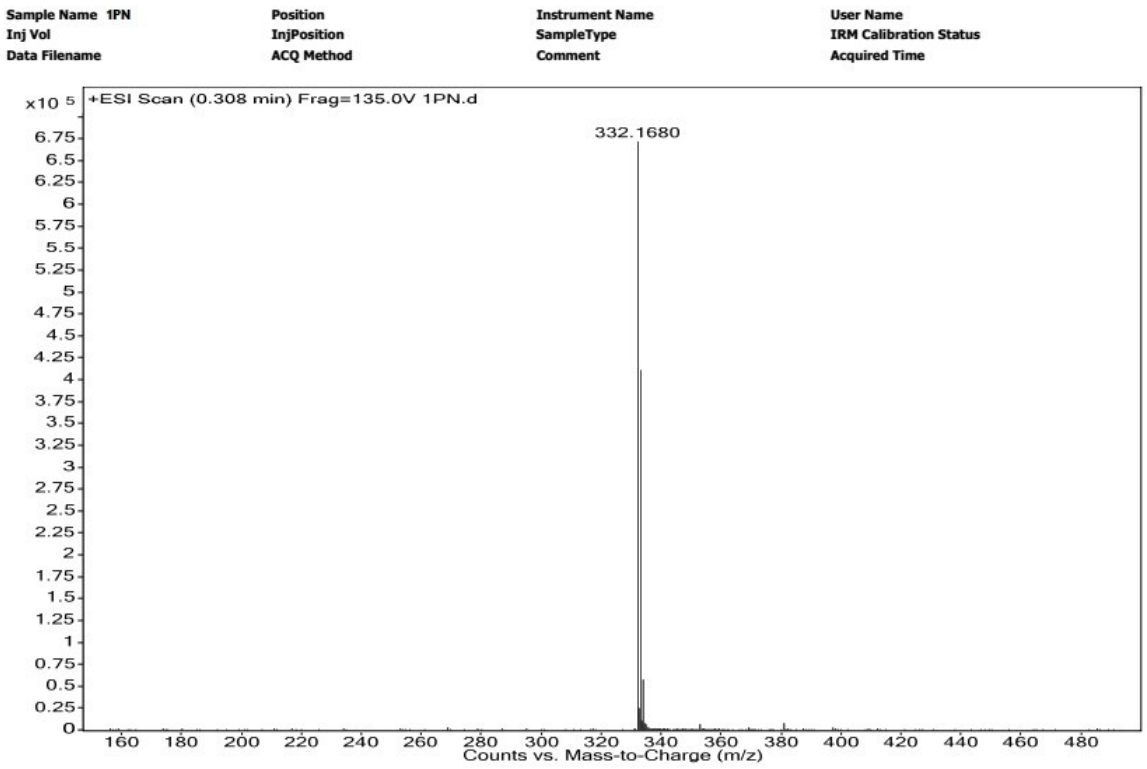

Fig. S10 HRMS of **1PN.**

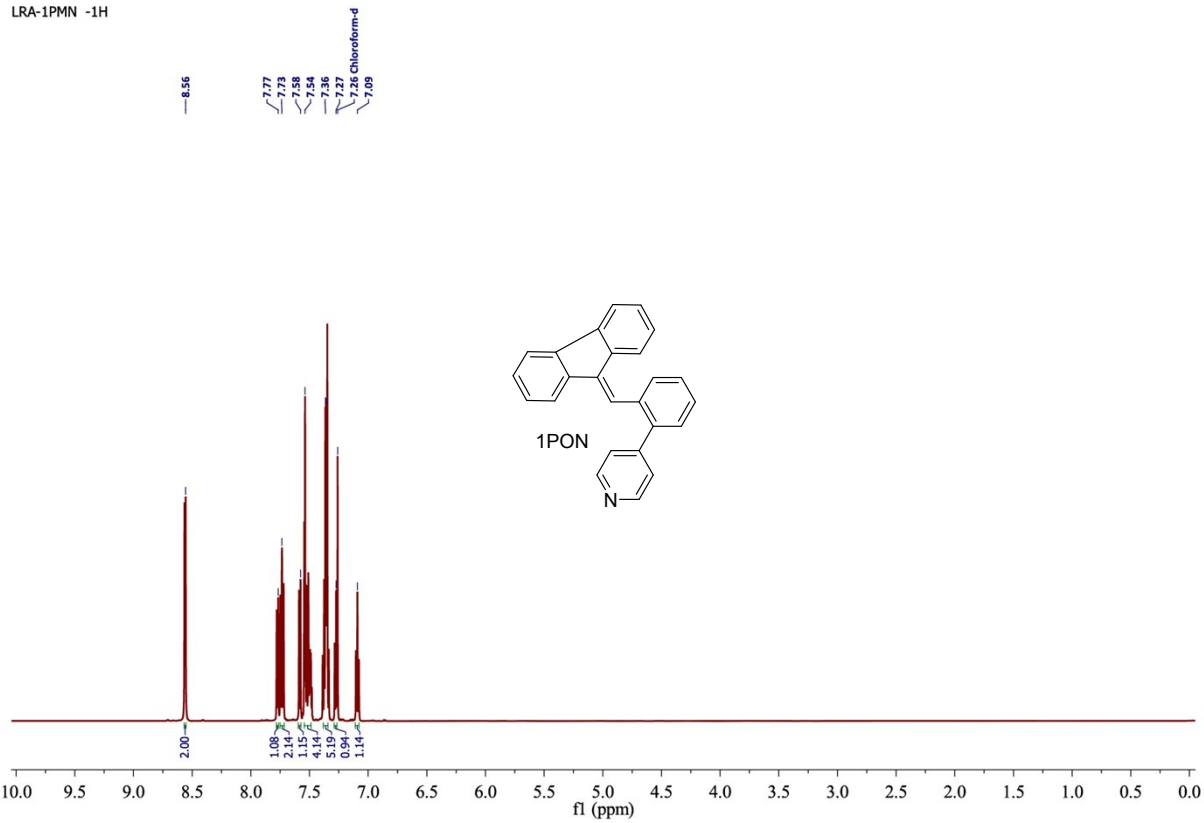

Fig. S11 ^{1}H NMR spectra of **1PON** in $CDCl_3$ solvent.

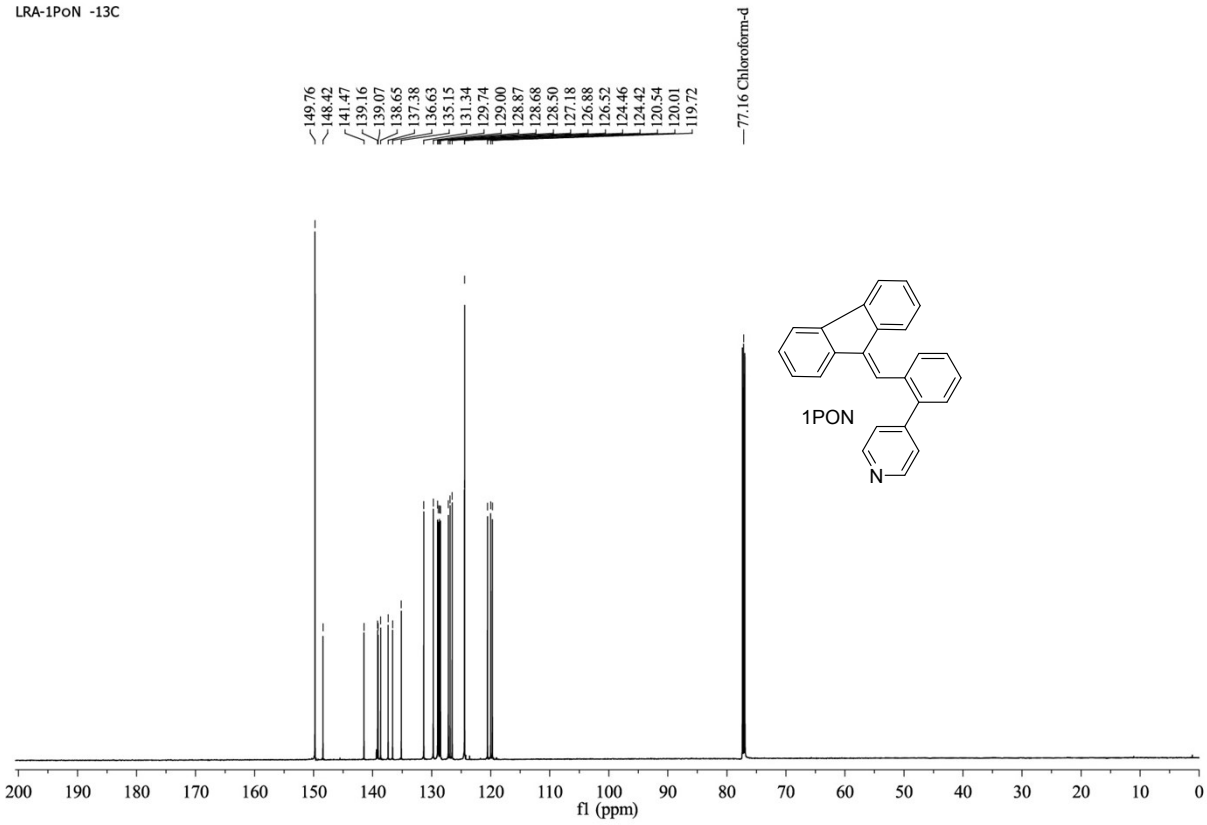

Fig. S12 ^{13}C NMR spectra of **1PON** in $CDCl_3$ solvent.

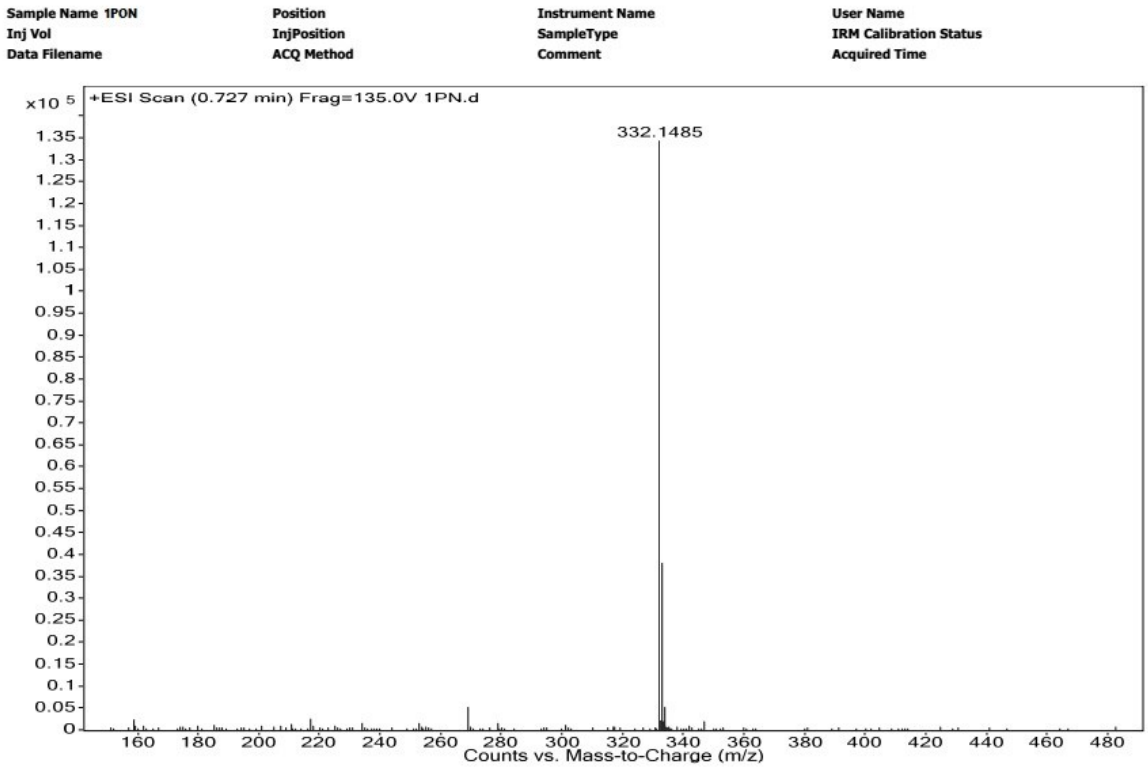

Fig. S13 HRMS spectra of **1PON.**

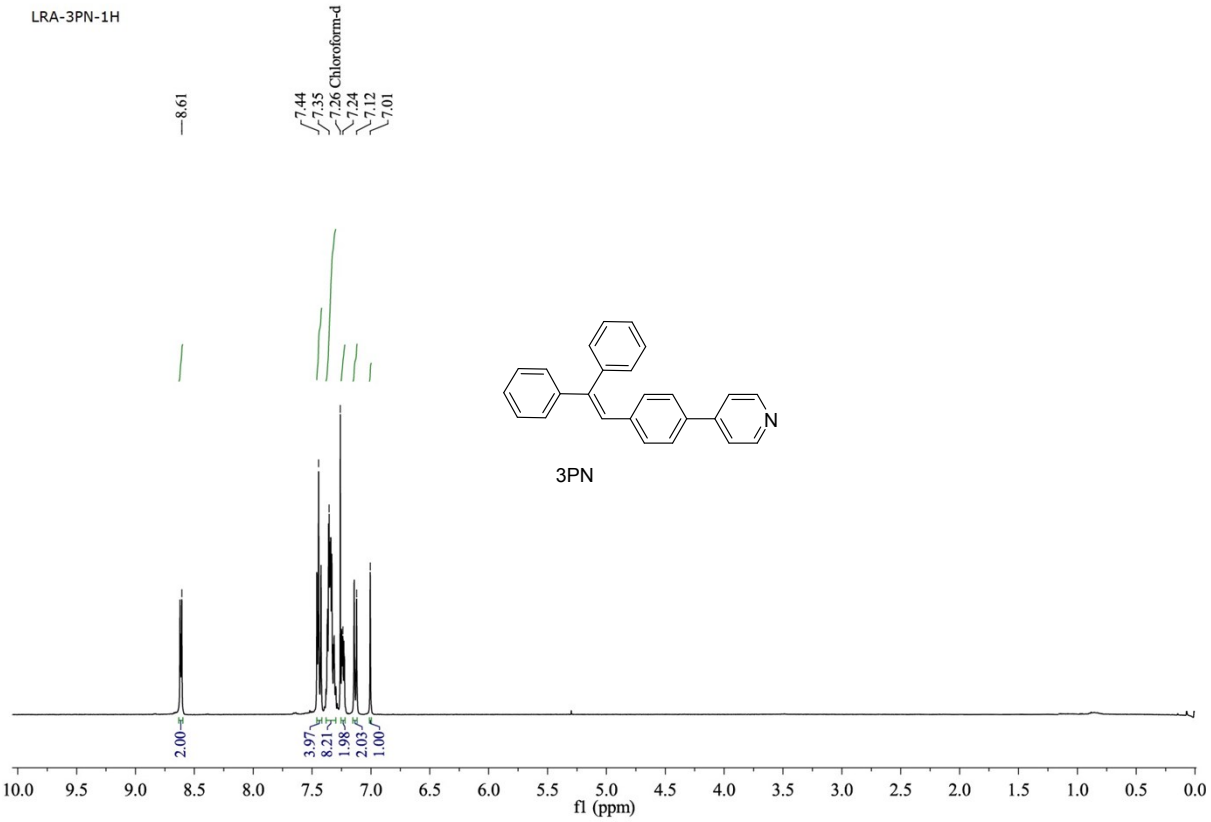

Fig. S14 ^{1}H NMR spectra of **3PN** in $CDCl_3$ solvent.

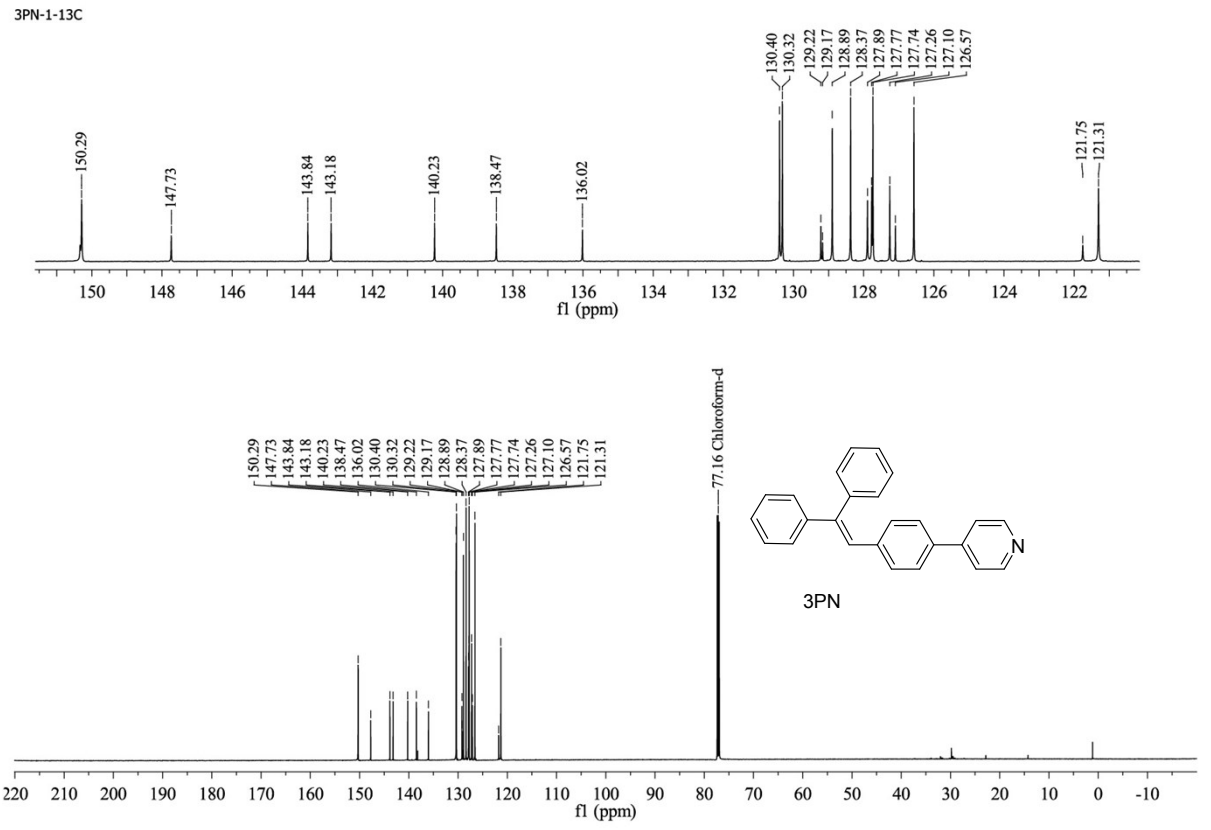

Fig. S15 ^{13}C NMR spectra of **3PN** in $CDCl_3$ solvent.

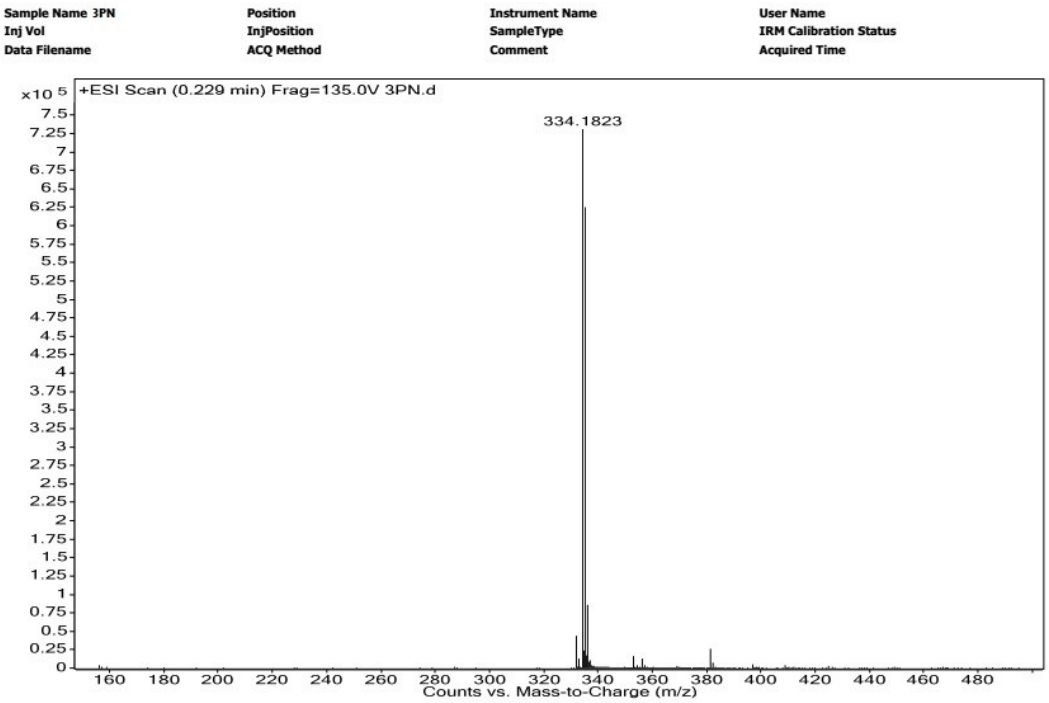

Fig. S16 HRMS spectra of **3PN**.

6. Photophysical studies

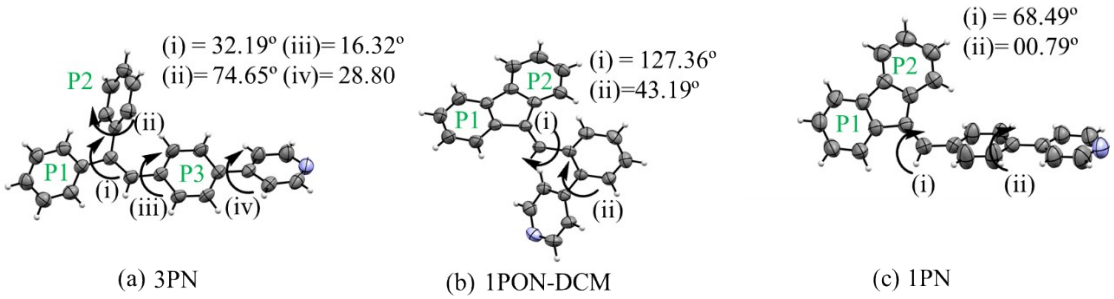

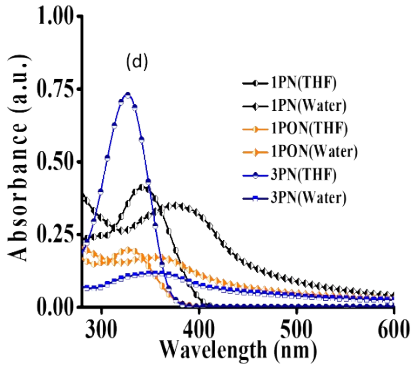

Fig. S17 Torsion angle of (a) 3**PN**, (b) **1PON** and (c) 1**PN** and (d) UV-vis. spectra of PN derivatives in THF, 99% f_w in room temperature.

Table S1 1PN, **1PON** and **3PN** (a) UV-vis. spectra in THF, 99% f_w & (b) PL spectra in THF, 99% f_w, and as solid film, quantum yield in 99% f_w at room temperature at 10 µM concentration. [a]Quinine sulfate in 0.1 M H_2SO_4 (reference). [b] fluorescence was very low therefore quantum yield could not measure.

Compound	λ_{max} abs (nm) THF	λ_{max} abs (nm) H_2O	λ_{max} PL (nm) THF	λ_{max} PL (nm) H_2O (99% f_w)	λ_{max} PL (nm) Solid	Φ_f[a] (%) THF	Φ_f[a] (%) H_2O
1PN	343	379	403,520	419,503	389,492	b	b
1PON	329	358	406,528	388,500	507	b	11.6
3PN	326	354	428	450	464	b	73.2

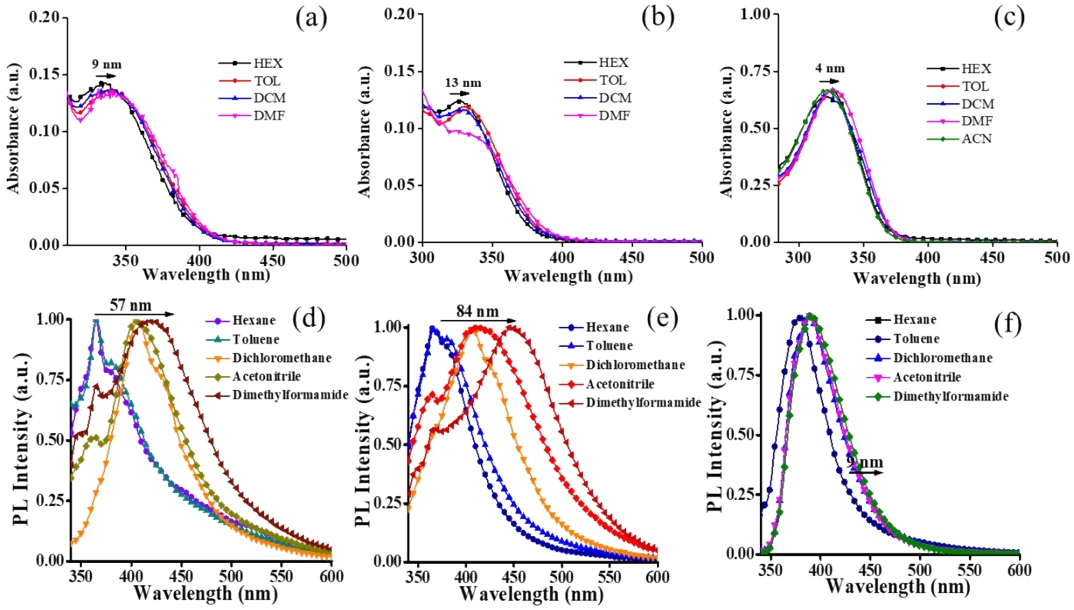

Fig. S18 UV vis. (a) **1PN** (b) **1PON** (c) **3PN** and PL spectra of (d) **1PN** (e) **1PON** (f) **3PN** in different polar solvents, all spectra were taken at room temperature.

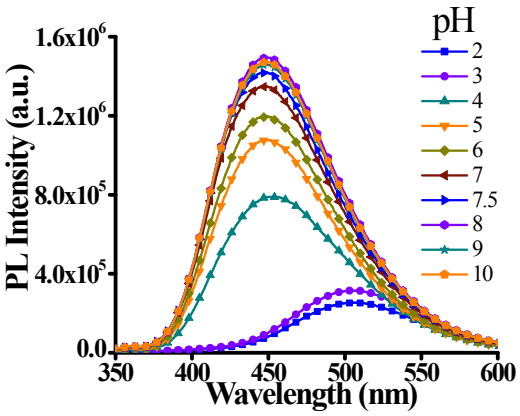

Fig. S19 PL spectra of **3PN** in different pH medium, all spectra were taken at room temperature.

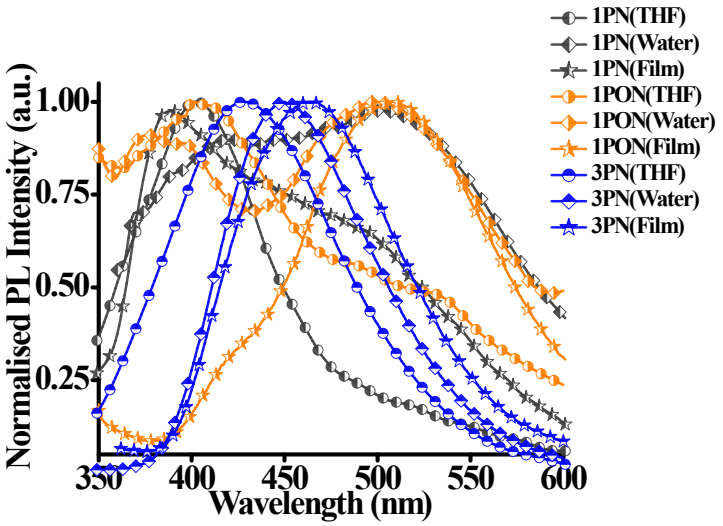

Fig. S20 PL spectra **1PN**, **1PON** and **3PN** in THF, 99% f_w and in the solid film at room temperature.

7. Quantum yield calculations for PN derivatives

The quantum yield (Φ_s) of **PN** derivatives were calculated in aqueous medium by using following equation, & quinine sulfate (Φ_s = 0.57 in 0.1 M H_2SO_4) was taken as reference dye.

$$\Phi_s = \Phi_r (A_r F_s / A_s F_r) (\eta_s^2 / \eta_r^2) \text{..... Equation-1}$$

Where, s and r represent sample and reference, Φ signifies the quantum yield, A denotes absorbance, F signifies relative integrated fluorescence intensity, and η represents the refractive index of the medium.

8. Studies of PN derivatives nanoparticles formation

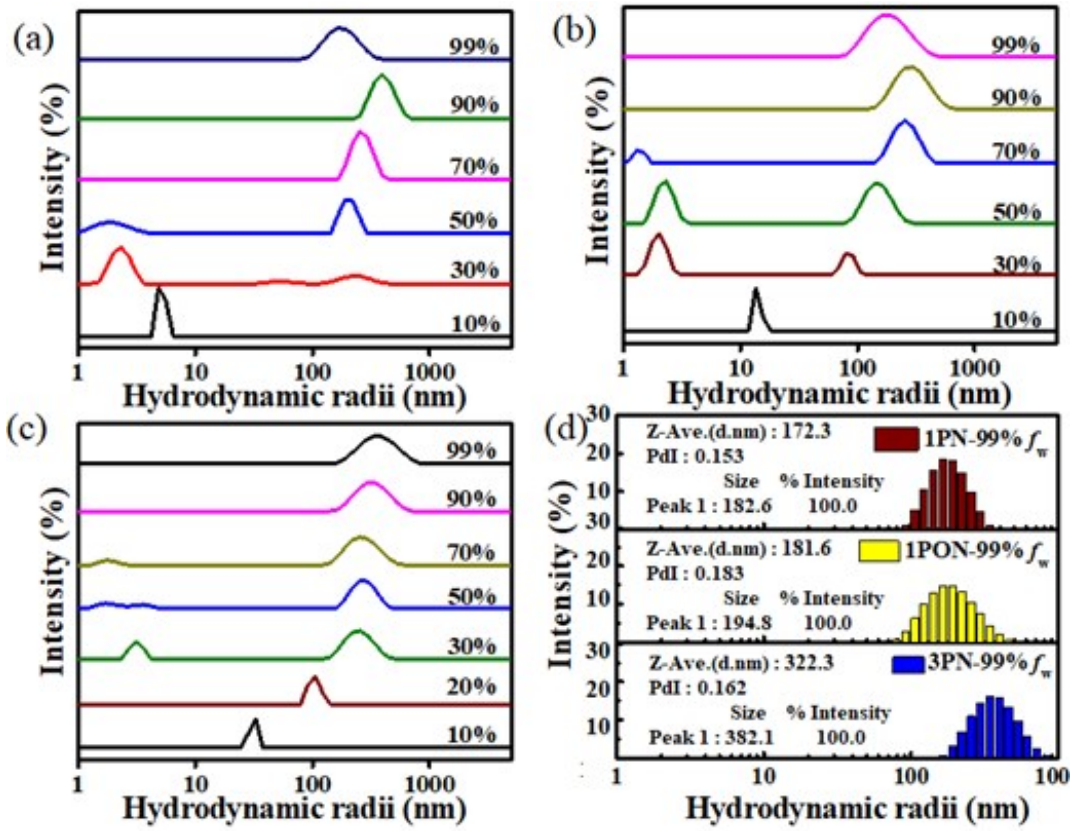

Fig. S21 Study of nanoparticle formation of PN derivatives by DLS spectroscopy with increasing %f_w in THF (a) **1PN** (b) **1PON** (c) **3PN**. (d) Average nanoparticle size in the 99% f_w at room temperature (10 μM solution).

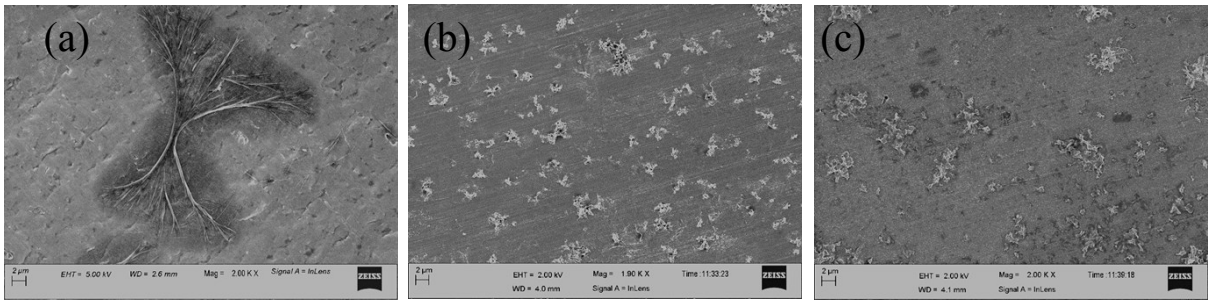

Fig. S22 FESEM images of (a) **1PN** (b) **1PON** (c) **3PN** nanoparticles formed in 99% f_w by simple drop-casting technique (10 μM).

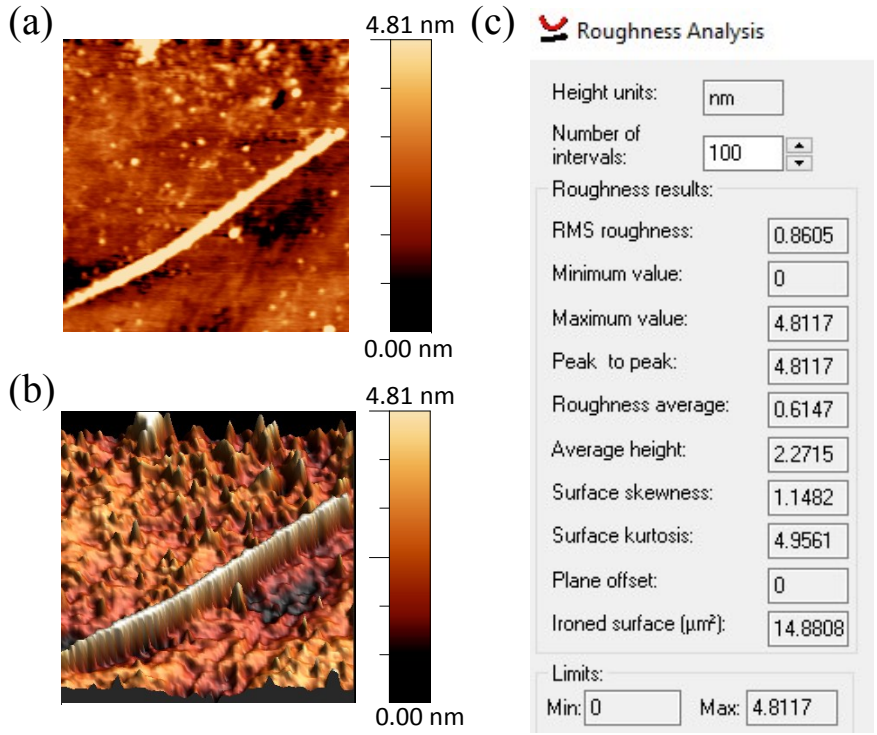

Fig. S23 AFM images of **1PN** derivative nanoparticles formed in 99% f_w by simple drop-casting on glass slide (10 µM).

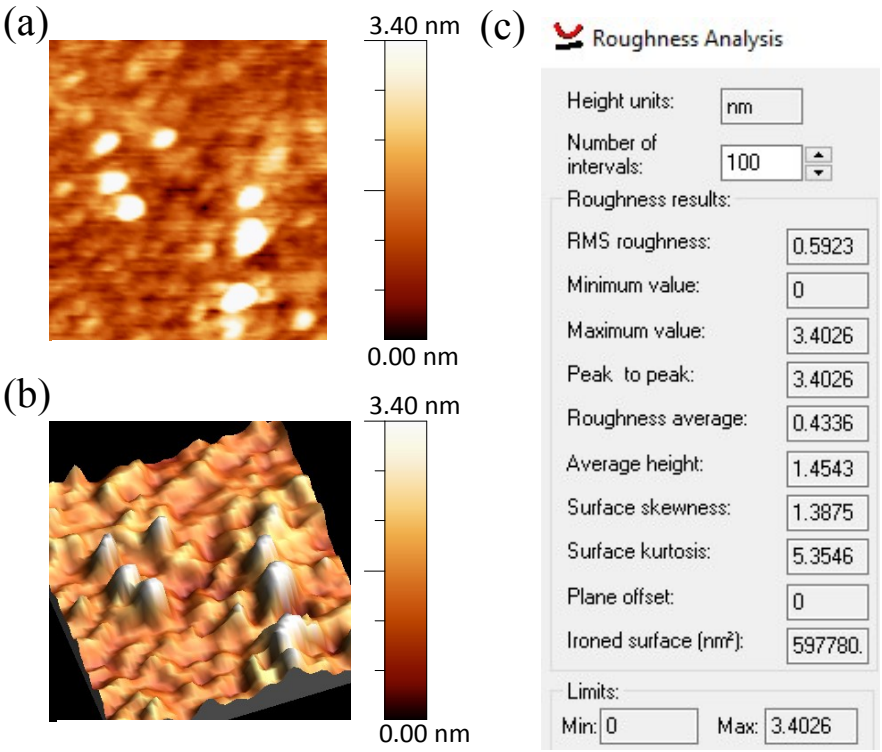

Fig. S24 AFM images of **1PON** derivative nanoparticles formed in 99% f_w by simple drop-casting on glass slide (10 µM).

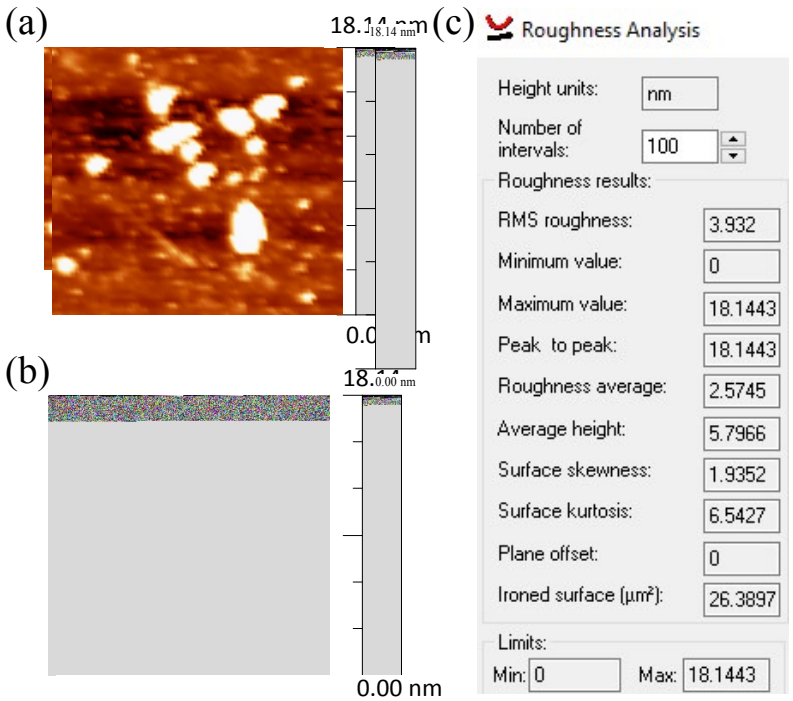

Fig. S25 AFM images of **3PN** derivative nanoparticles formed in 99% f_w by simple drop-casting on glass slide (10 µM).

9. Theoretical studies

In order to elucidate the electronic distribution, theoretical studies were performed using Gaussian 09W software[1]

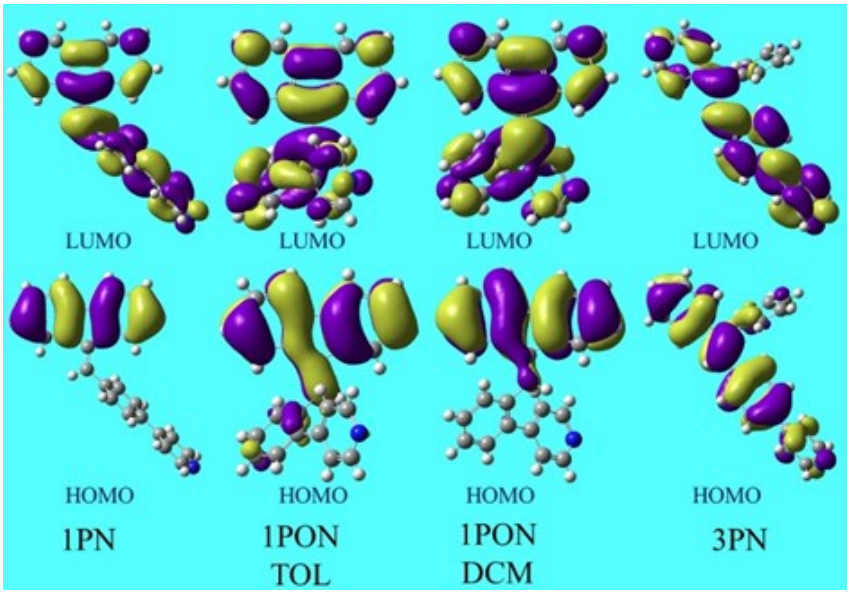

Fig. S26 Frontier molecular orbitals (FMO) amplitude plots of **1PN, 1PON_Tol, 1PON_DCM** and **3PN** calculated by B3LYP/6-31G(d, p).

10. Molecular packing and arrangement

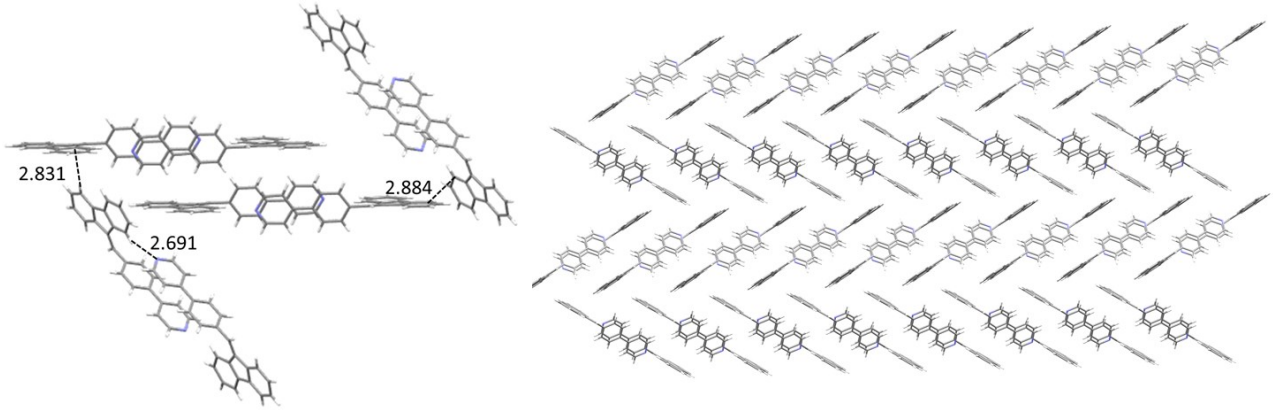

Fig. S27 1PN molecular packing and arrangement from SCXRD.

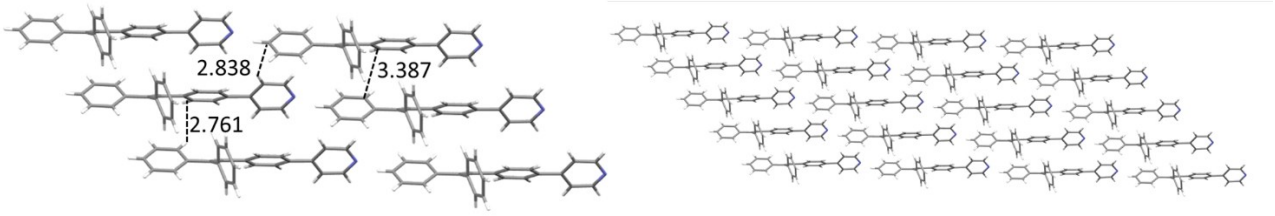

Fig. S28 3PN molecular packing and arrangement from SCXRD.

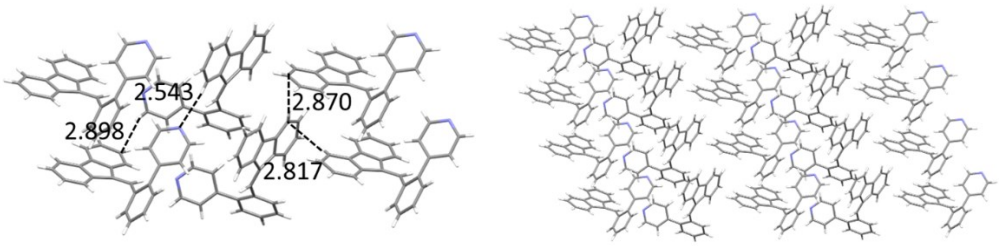

Fig. S29 1PON_Tol molecular packing and arrangement from SCXRD.

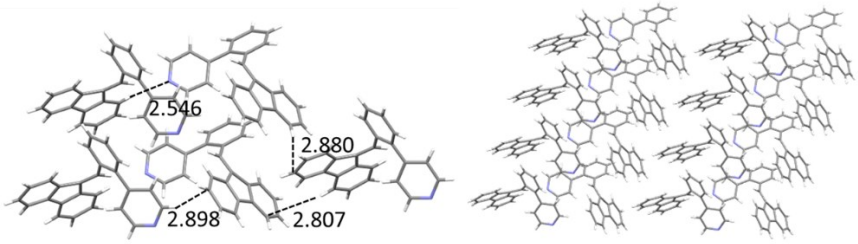

Fig. S30 1PON_DCM molecular packing and arrangement from SCXRD.

Table S2. Single crystal X-ray diffraction data of **1PN**.

S No.	Compound	1PN
1	Empirical formula	C_{25} H_{17} N
2	CCDC NO	1850300
3	Formula weight	331.40
4	Temperature/K	298 K
5	Crystal system	Monoclinic
6	Space group	P2(1)/c
7	a/Å	8.3412(4)
8	b/Å	20.3704(9)
9	c/Å	10.3467(5)
10	α/°	90.00
11	β/°	95.383(3)
12	γ/°	90.00
13	Volume/Å^3	1750.29(14)
14	Z	4
15	ρ**calc**mg/mm^3	1.258
16	m/mm^{-1}	0.073
17	F(000)	696.00
18	Crystal size/mm^3	0.28 × 0.23 × 0.17
19	2Θ range for data collection	2.00 to 47.78°
20	Index ranges	$-9 \leq h \leq 9$, $-24 \leq k \leq 24$, $-12 \leq l \leq 12$
21	Reflections collected	18868
22	Independent reflections	3102[R(int) = 0.0432]
23	Data/restraints/parameters	3102/0/235
24	Goodness-of-fit on F2	0.954
25	Final R indexes [I>=2σ(I)]	R1 = 0.0508, wR2 = 0.1366
26	Final R indexes [all data]	R1 = 0.0975, wR2 = 0.1670

Table S3. Single crystal X-ray diffraction data of **3PN**.

S No.	Compound	3PN
1	Empirical formula	C_{25} H_{19} N
2	CCDC NO	1850519
3	Formula weight	333.41
4	Temperature/K	296 K
5	Crystal system	Monoclinic
6	Space group	P 21/n
7	a/Å	5.7544(7)
8	b/Å	11.1791(13)
9	c/Å	28.221(3)
10	α/°	90.00
11	β/°	95.062(2)
12	γ/°	90.00
13	Volume/Å^3	1808.4(4)
14	Z	4
15	ρ**calc**mg/mm^3	1.225
16	m/mm^{-1}	0.071

17	F(000)	704
18	Crystal size/mm^3	0.26 × 0.21 × 0.15
19	2Θ range for data collection	1.44 to 25.00°
20	Index ranges	$-6 \leq h \leq 6$, $-13 \leq k \leq 13$, $-33 \leq l \leq 33$
21	Reflections collected	58468
22	Independent reflections	58468 [R(int) =0.0379]
23	Data/restraints/parameters	58468/0/235
24	Goodness-of-fit on F2	1.078
25	Final R indexes [I>=2σ(I)]	R1 = 0.0388, wR2 = 0.1026
26	Final R indexes [all data]	R1 = 0.0474, wR2 = 1.078

Table S4. Single crystal X-ray diffraction data of **1PON**_Toluene.

S No.	Compound	1PON_Toluene
1	Empirical formula	C_{25} H_{17} N
2	CCDC NO	1938858
3	Formula weight	331.39
4	Temperature/K	296 K
5	Crystal system	Monoclinic
6	Space group	P21/n
7	a/Å	16.8262(9)
8	b/Å	6.0687(3)
9	c/Å	18.6754(10)
10	α/°	90.00
11	β/°	110.396(6)
12	γ/°	90.00
13	Volume/Å^3	1787.45(17)
14	Z	4
15	ρ**calc**mg/mm^3	1.231
16	m/mm^{-1}	0.071
17	F(000)	696
18	Crystal size/mm^3	0.34 × 0.21 × 0.13
19	2Θ range for data collection	2.327 to 28.948 °
20	Index ranges	$-22 \leq h \leq 9$, $-8 \leq k \leq 5$, $-24 \leq l \leq 24$
21	Reflections collected	7893
22	Independent reflections	4110[R(int) = 0.0269]
23	Data/restraints/parameters	7893/0/235
24	Goodness-of-fit on F2	1.080
25	Final R indexes [I>=2σ(I)]	R1 = 0.0552, wR2 = 0.1129
26	Final R indexes [all data]	R1 = 0.0988, wR2 = 0.1382

Table S5. Single crystal X-ray diffraction data of **1PON**_DCM.

S No.	Compound	1PON (DCM)
1	Empirical formula	C_{25} H_{17} N
2	CCDC NO	1941127
3	Formula weight	331.39

4	Temperature/K	296 K
5	Crystal system	Monoclinic
6	Space group	P21/n
7	a/Å	16.8722(15)
8	b/Å	6.0689(4)
9	c/Å	18.7149(19)
10	α/°	90.00
11	β/°	110.549(11)
12	γ/°	90.00
13	Volume/Å^3	1794.4(3)
14	Z	4
15	ρ**calc**mg/mm^3	1.227
16	m/mm^{-1}	0.071
17	F(000)	696
18	Crystal size/mm^3	0.30 × 0.24 × 0.17
19	2Θ range for data collection	3.54 to 25.75°
20	Index ranges	-9 ≤ h ≤ 20, -7 ≤ k ≤ 6, -22 ≤ l ≤ 21
21	Reflections collected	6493
22	Independent reflections	1982[R(int) = 0.0345]
23	Data/restraints/parameters	6493/0/235
24	Goodness-of-fit on F2	1.185
25	Final R indexes [I>=2σ(I)]	R1 = 0.0832, wR2 = 0.2526
26	Final R indexes [all data]	R1 = 0.1180, wR2 = 0.3373

11. Mechanoresonsive studies of PDMS film

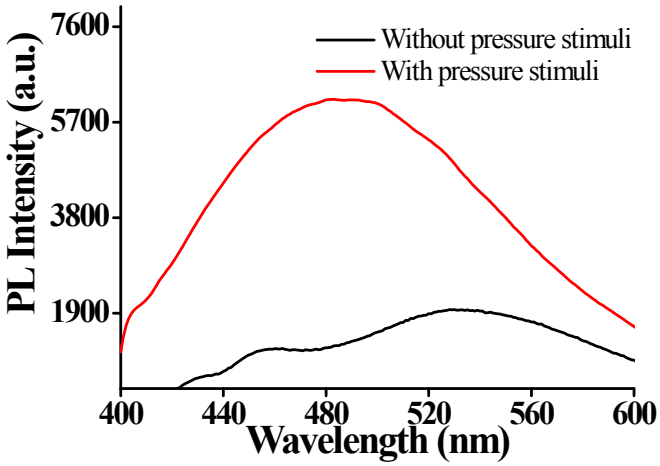

Fig. S31 Enhancement of emission of PDMS thin film after pressure stimuli**.**

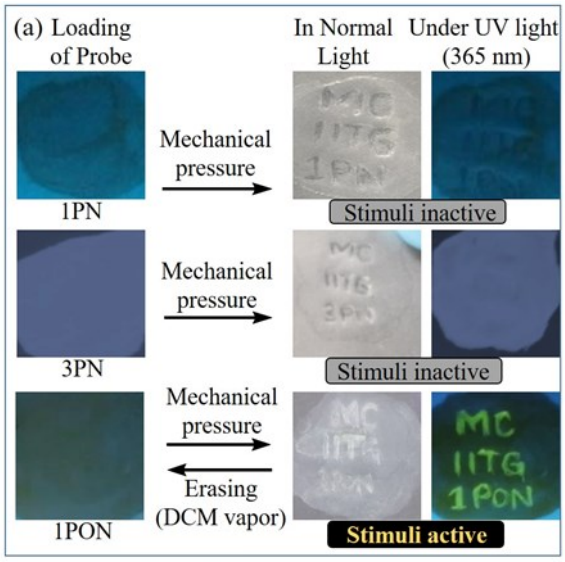

Fig. S32 Mechanochromic emission study of **PN** derivatives in weighing paper and developing erasable secret ink using **1PON**.

12. Sensing of CWA and limit of detection calculation

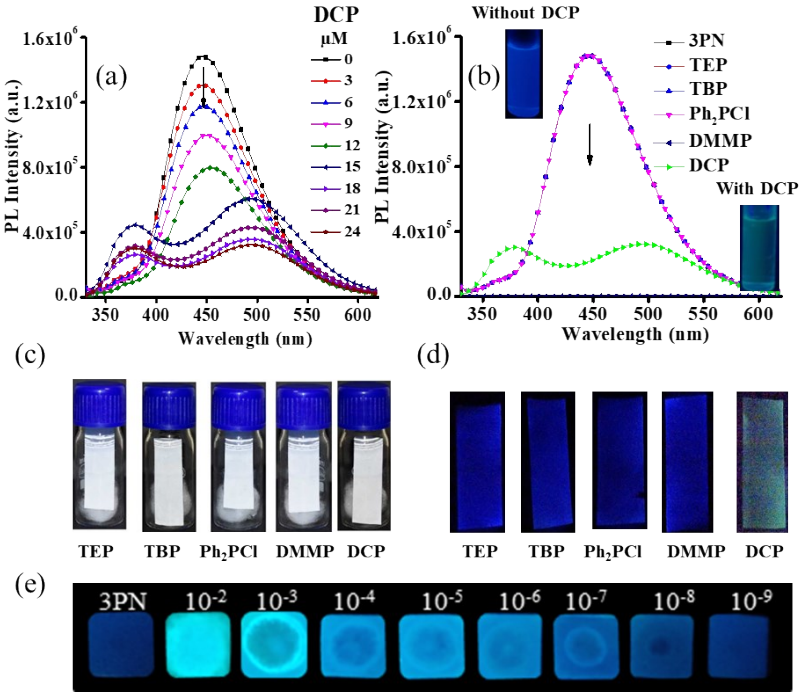

Fig. S33 (a) PL spectra of **3PN** (10 μM) in 99% fw upon gradual addition of DCP (0-24 μM) (b) PL spectra of **3PN** 99% fw after addition of different guest analytes (30 μM). Portable device made by **3PN** dipped Whatman filter paper for sensing CWAs vapors and similar analytes (100 μM) exposed (1 min) in (c) normal light (d) UV lamp (e) Whatman filter paper based device pictures sensing various CWA concentration by 3PN under UV lamp.

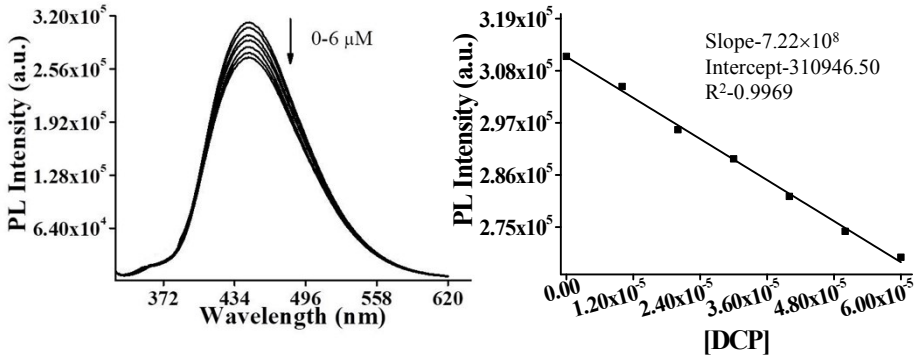

Fig. S34 Change of fluorescence intensity of **3PN** in lower concentration of DCP in 99% f_w.

$$LOD = 3 \times S.D. / k$$

$$LOD \text{ for DCP} = 3 \times 1653.90 / 7.22 \times 10^8$$

$$= 70.88 \times 10^{-7} \text{ M}$$

13. Determination of nerve agents sensing mechanism by 3PN

3PN fluorescence response towards DCP is due to the pyridine group because it has stronger nucleophilicity (pKa = 5.17). Hence the pyridine group will be first electrophilically attacked by the phosphonyl group of DCP, forming an unstable intermediate, whose N–P bond is further attacked easily by a weak nucleophilic reagent like oxygen atoms from H_2O (either form the aqueous medium or from vapor) ultimately to be rapidly hydrolyzed into pyridinium salt. As a result, fluorescence changes due to push–pull electron effect can be observed. Meanwhile, the nerve agent mimic DCP will transform into non-toxic neutral phosphate. This sensing mechanism was confirmed by ^{1}H NMR.

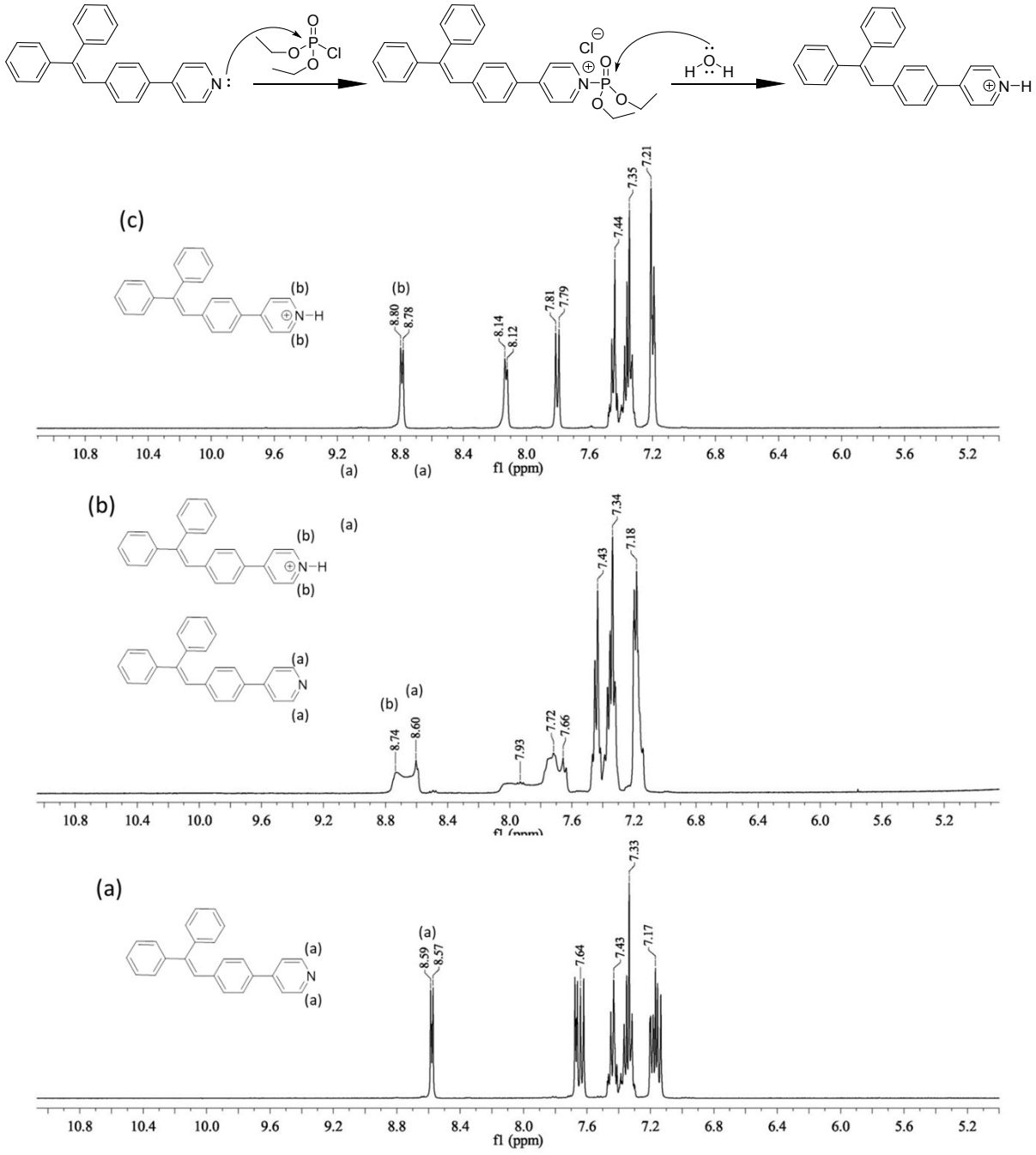

Fig. S35. Proposed mechanism of sensing and shift of ^{1}H NMR peaks of **3PN** in (a) absence of DCP (b) 0.5 equivalent of DCP (c) 1 equivalent of DCP in DMSO-d_6 solvent.

14. Reference

1 M. J. Frisch, G. W.Trucks, H. B. Schlegel, G. E. Scuseria, M. A. Robb, J. R. Cheeseman, G. Scalmani, V. Barone, B. Mennucci, G. A. Petersson, H. Nakatsuji, M. Caricato, X. Li, H. P. Hratchian, A. F. Izmaylov, J. Bloino, G. Zheng, J. L. Sonnenberg, M. Hada, M. Ehara, K. Toyota, R. Fukuda, J. Hasegawa, M. Ishida, T. Nakajima, Y. Honda, O. Kitao, H. Nakai, T. Vreven, J. A. Montgomery, J. E., Jr. Peralta, F. Ogliaro, M. Bearpark, J. J. Heyd, E. Brothers, K. N. Kudin, V. N. Staroverov, T. Keith, R. Kobayashi, J. Normand, K. Raghavachari, A. Rendell, J. C. Burant, S. S. Iyengar, J. Tomasi, M. Cossi, N. Rega, J. M. Millam, M. Klene, J. E. Knox, J. B. Cross, V. Bakken, C. Adamo, J. Jaramillo, R. Gomperts, R. E.Stratmann, O. Yazyev, A. J. Austin, R. Cammi, C. Pomelli, J. W. Ochterski, R. L. Martin, K. Morokuma, V. G. Zakrzewski, G. A. Voth, P. Salvador, J. J. Dannenberg, S. Dapprich, A. D. Daniels, O. Farkas, J. B. Foresman, J. V. Ortiz, J. Cioslowski, D. J. Fox, Gaussian 09; Gaussian, Inc.: Wallingford CT, 2013.